

# Nanoscale

Accepted Manuscript



This is an *Accepted Manuscript*, which has been through the Royal Society of Chemistry peer review process and has been accepted for publication.

*Accepted Manuscripts* are published online shortly after acceptance, before technical editing, formatting and proof reading. Using this free service, authors can make their results available to the community, in citable form, before we publish the edited article. We will replace this *Accepted Manuscript* with the edited and formatted *Advance Article* as soon as it is available.

You can find more information about *Accepted Manuscripts* in the [Information for Authors](#).

Please note that technical editing may introduce minor changes to the text and/or graphics, which may alter content. The journal's standard [Terms & Conditions](#) and the [Ethical guidelines](#) still apply. In no event shall the Royal Society of Chemistry be held responsible for any errors or omissions in this *Accepted Manuscript* or any consequences arising from the use of any information it contains.

---

# Microsphere Assembly of TiO<sub>2</sub> Mesoporous Nanosheets with Highly Exposed (101) Facets and Application in Light-Trapping Quasi-Solid-State Dye-Sensitized Solar Cell

Xiyun Tao<sup>1</sup>, Peng Ruan<sup>1</sup>, Xiang Zhang, Hongxia Sun, Xingfu Zhou \*

College of Chemistry and Chemical Engineering & State Key Laboratory of Material-Oriented Chemical Engineering, Nanjing Technology University, Nanjing 210009, P. R. China

\*Corresponding author: Tel: +86-25-83172270, Fax: +86-25-83172270,

E-mail address: Zhouxf@njut.edu.cn (Prof. X. F. Zhou)

**Abstract:** The morphology of nano-titania has a significant effect on photoelectric properties of dye-sensitized solar cells. In this paper, microsphere assembly of TiO<sub>2</sub> mesoporous nanosheet constructed by nanocuboids is synthesized via a simple hydrothermal process. XRD pattern indicates the hierarchical mesoporous microspheres are anatase phase with the decreased (004) peaks. Raman spectrum shows the enhanced E<sub>g</sub> peaks at 143 and 638 cm<sup>-1</sup> caused by symmetric stretching vibration of O–Ti–O of (101) crystalline facet in anatase TiO<sub>2</sub>. FESEM and TEM images show that the well monodispersed TiO<sub>2</sub> microspheres with a diameter of 2 μm are assembled by TiO<sub>2</sub> mesoporous nanosheets with exposed (101) facets. The oriented attachment of TiO<sub>2</sub> nanocuboids along the (101) direction leads to the formation of the mesoporous titania nanosheets. UV-Vis spectrum shows that microsphere assembly of mesoporous TiO<sub>2</sub> nanosheets has high scattering ability and light dye absorption. Quasi-solid-state dye-sensitized solar cells using these microspheres as the top scattering layers exhibits a prominent improvement in the power conversion efficiency of 7.51%, which shows a 45.8 percent increase in the overall conversion efficiency when compared with the spine hierarchical TiO<sub>2</sub> microspheres (5.15%). Study displays that microsphere assembly of mesoporous TiO<sub>2</sub> nanosheets has a potential application in quasi-solid-state dye-sensitized solar cells with an excellent stability.

**Keywords:** Mesoporous TiO<sub>2</sub> nanosheet; TiO<sub>2</sub> nanocuboids; microsphere; light-scattering; quasi-solid electrolyte; dye-sensitized solar cell

## 1. Introduction

As a renewable energy, the solar energy has the greatest potential, and it can be gained by direct or indirect methods.<sup>1</sup> The earliest solar cell emerged in 1839 in Becquerel laboratory and different types of cells based on monocrystalline, polycrystalline silicon and amorphous silicon have been developed immediately.<sup>2</sup> Dye-sensitized solar cell (DSSC), as a new photovoltaic device,<sup>3-5</sup> has been attracting extensive attention due to its unique advantages of low-cost, high efficiency of converting light to electricity, environmental friendly and ease of preparation processing.<sup>6-9</sup> To obtain a higher efficiency, each part of DSSC, including dye, photoanode, counter electrodes and electrolytes has been studied in-depth.<sup>10-13</sup> Because of the stable chemical properties and a better combination with dye, TiO<sub>2</sub> is most suitable for the preparation of DSSCs among number of the semiconductor materials.<sup>14</sup> TiO<sub>2</sub> is the main part of the photoanode, playing a role of loading dye, collecting and transmitting electron.

As the core of the DSSCs, the optimizing of photoanode is never stopped by researchers. With the development of science and technology, the investigation of the microcosmic structure of TiO<sub>2</sub> is deeper. To enhance the photocurrent of DSSCs, different morphologies are synthesized, such as TiO<sub>2</sub> nanowires,<sup>15,16</sup> nanotubes,<sup>17,18</sup> nanorods<sup>19,20</sup> and nanospheres.<sup>21,22</sup> Generally speaking, superior photoanode film should comprise four main characteristics:<sup>23</sup> specific crystalline facet, high surface area, the effective electron transport and the high light-scattering ability. Dye molecules adhered to the surface of TiO<sub>2</sub> film by physical adsorption, TiO<sub>2</sub> film can absorb more dye if it has a highly exposed (101) facets and high surface area. Thus, the photoanode can absorb more sunlight.<sup>24</sup> Compared to the disorganized polycrystalline interface, the electrons have an efficient transfer in one-dimensional or crystal interface of the TiO<sub>2</sub> film, which improves the electron transport efficiency of the DSSCs.<sup>25</sup> In addition, the introduction of light-scattering layer on TiO<sub>2</sub> film can capture sunlight efficiently by increasing the optical path and reducing the loss of light, also resulting in an increase in photocurrent.<sup>26</sup> Fang et al<sup>27</sup> obtained a higher photoelectric conversion efficiency after introducing anatase TiO<sub>2</sub> microspheres as the top light-scattering layer.

Electrolyte is an integral part of the sandwich structure in DSSCs. The liquid electrolyte is used by researchers in most of the study of DSSCs.<sup>28</sup> Quasi-solid electrolyte has the advantages of less volatile and high stability compared with the traditional liquid electrolyte. However, the quasi-solid electrolyte has a disadvantage of low photoelectric conversion efficiency. This is mainly due to poor electron migration of oxidation-reduction in a higher viscosity of the solid electrolyte. Besides, the electron

transport impedance between photoanode and electrolyte interface is larger. A few researchers have been carried out the study of new and efficient quasi-solid-state dye-sensitized solar cells. Kang<sup>29</sup> used polyoxyethylene PEO and nano-crystalline TiO<sub>2</sub> in the quasi-solid electrolyte. Dai<sup>30</sup> prepared quasi-solid electrolyte by adding the gelling agent of liquid crystal (4 - cyano-4'-heptyloxy biphenyl) into the traditional liquid electrolyte and obtained a high-efficiency quasi-solid DSSC.

Herein, we synthesize the microsphere assembly of mesoporous TiO<sub>2</sub> nanosheet constructed with nanocuboids by hydrothermal route. XRD data indicates the hierarchical mesoporous microspheres are anatase TiO<sub>2</sub>. FESEM and TEM show the hierarchical microflowers are monodispersed and formed by spine shaped TiO<sub>2</sub> mesoporous nanosheets, which are further constructed with 10 nm in width and 20 nm in length TiO<sub>2</sub> nanocuboids with exposed (101) facets. UV-Vis tests show that the microspheres have a high light scattering and dye adsorption ability. Quasi-solid-state DSSC using microsphere assembly of mesoporous TiO<sub>2</sub> nanosheet as the scattering layers exhibited a prominent improvement in the power conversion efficiency.

## 2. Experimental Section

**Materials and Reagents:** All chemicals were analytical-grade reagents and used as originally received without further purification. Tetrabutyl titanate and acetonitrile were obtained from Shanghai Lingfeng Reagent Co., Ltd (China). Acetic acid and hydrofluoric acid were obtained from Shanghai Shenbo Chemical Co., Ltd (China). Lithium iodide and 4-tert-butylpyridine (TBP) were purchased from Shanghai Jingchun Reagent Co., Ltd (China). 1,3-dimethyl-imidazolium iodide and guanidine thiocyanate was obtained from Dalian Rainbow Light Solar Technology Development Co., L(China). Ethanol was obtained from Wuxi Yasheng Chemical Co., Ltd (China). Iodine was obtained from Shanghai Shisihewei Chemical Co., Ltd (China). 4-cyano-4' heptyloxy biphenyl (LC) was purchased from Alfa Aesar. The water used in this experiment was deionized water.

**Fabrication of microsphere assembly of mesoporous TiO<sub>2</sub> nanosheets:** 1.0 mL of tetrabutyl titanate was dissolved in 30 mL of acetic acid slowly with agitation for 10 min at the room temperature. The mixture was transferred into a Teflon-lined stainless steel autoclave (80 mL capacity). The autoclave was sealed and maintained at 423 K for 12 h in the oven and then cooled to ambient temperature naturally. After the hydrothermal reaction, the precipitate in the bottom of the autoclave was collected. The precipitate was washed with deionized water twice, and then washed with ethanol. After

purification with deionized water and ethanol, the sample was dried in the oven at 353 K in air atmosphere. The product was further calcined at 773 K for 2 h.

**Fabrication of quasi-solid-state DSSCs:** The fluorine-doped tin oxide (FTO) glass substrate was cleaned with detergents, deionized water and absolute ethanol in an ultrasonic cleaning instrument, respectively, then treated with 40 mM  $\text{TiCl}_4$  aqueous solution at 343 K for 30 min. A certain amount of  $\text{TiO}_2$  powder was mixed with ethyl cellulose and dispersed in a mixed ethanol and terpineol solution. The mixture was ground in an agate mortar for at least 30 minutes to prepare a screen-printable  $\text{TiO}_2$  paste. Subsequently, the paste was deposited onto the FTO glass by using screen-printed method, followed by a sintering of the program process. Afterwards, glass coated with  $\text{TiO}_2$  was immersed in aqueous solution containing 40 mM  $\text{TiCl}_4$  at 343 K for 30 min to obtain a modified film before sintering at 723 K for 30 minutes again. When the calcinations are finished, the film was cooled down to 353 K and immersed into 0.3 mM ethanol solution of N-719 dye for 24 h. After that, the dye-sensitized film was washed by ethanol immediately and dried in the oven at 353 K. The solar cell was assembled into a sandwich-type device by placing a Pt/FTO counter electrode on the dye-sensitized photoanode separated by a hot-melt gasket. For the preparation of quasi-solid-state electrolyte, 0.1 M iodine and 1 M 1,3-dimethyl-imidazolium iodide (DMII) and 0.5 M 4-tert-butyl-pyridine (TBP) and 0.1 M lithium iodide were added into acetonitrile solution in turn and stirred to form a homogeneous solution. 4-cyano-4'-heptyloxy biphenyl was added to the above liquid electrolyte and the mass fraction of 4-cyano-4'-heptyloxy biphenyl was 30%. The final solution was uniformly dissolved with ultrasound. The quasi-solid electrolyte was dissolved by heating and injected through the hole drilled on the Pt counter electrode. The hole was sealed using a hot-melt gasket at last.

**Characterization and Analysis:** The product was performed by powder X-ray diffraction (XRD) measurements on a Bruker-D8Advance X-ray diffractometer, with monochromatized  $\text{Cu K}\alpha$  incident radiation ( $\lambda = 1.5418 \text{ \AA}$ ) at 40 kV and 40 mA. The XRD patterns were recorded for  $2\theta$  value in the range of  $20^\circ$ - $80^\circ$  with a scanning increment of  $0.05^\circ$  at a scan speed of  $0.2^\circ$  second per step. The Horiba Jobin-Yvon LabRAM ARAMIS Raman spectrometer was used to characterize the Raman spectra of the sample with 532 nm-wavelength laser. The scanning electron microscopy (SEM, FEI, Quanta 200) and Field Emission scanning electron microscopy (FE-SEM, Hitachi S-4800) with an acceleration voltage of 30 kV was used to investigate the morphology of the samples, Transmission electron microscopy (TEM) and high-resolution transmission electron microscopy (HR-TEM) was

carried out on a JEM-2010UHR instrument (JEOL, Japan), using an acceleration voltage of 200 kV.

The photocurrent-voltage characteristics of the quasi-solid-state DSSCs were measured by a Newport oriel solar simulator and Keithley 2420 source meter (USA) under AM 1.5G simulator solar light with an illumination intensity of  $100\text{mW cm}^{-2}$ . Before the measurement, the solar simulator was calibrated using a standard silicon solar cell. The active area of the quasi-solid DSSCs was  $0.16\text{ cm}^2$ . Electrochemical impedance spectroscopy (EIS) measurements of the quasi-solid DSSCs were recorded by the electrochemical workstation (CHI660C, CH Instruments) under  $100\text{ mW/cm}^2$  illumination. we immersed the dye-absorbed  $\text{TiO}_2$  film into 10ml of 0.1M NaOH solution in the water and ethanol mixture with a volume ratio of 1:1 overnight and measured the concentration of the desorbed dye by a Perkin-Elmer UV/Vis spectrophotometer (model Lambda 950), and the diffuse-reflectance, absorbance spectra of the  $\text{TiO}_2$  films were recorded on the same UV/Vis spectrophotometer synchronically.

### 3. Result and Discussion

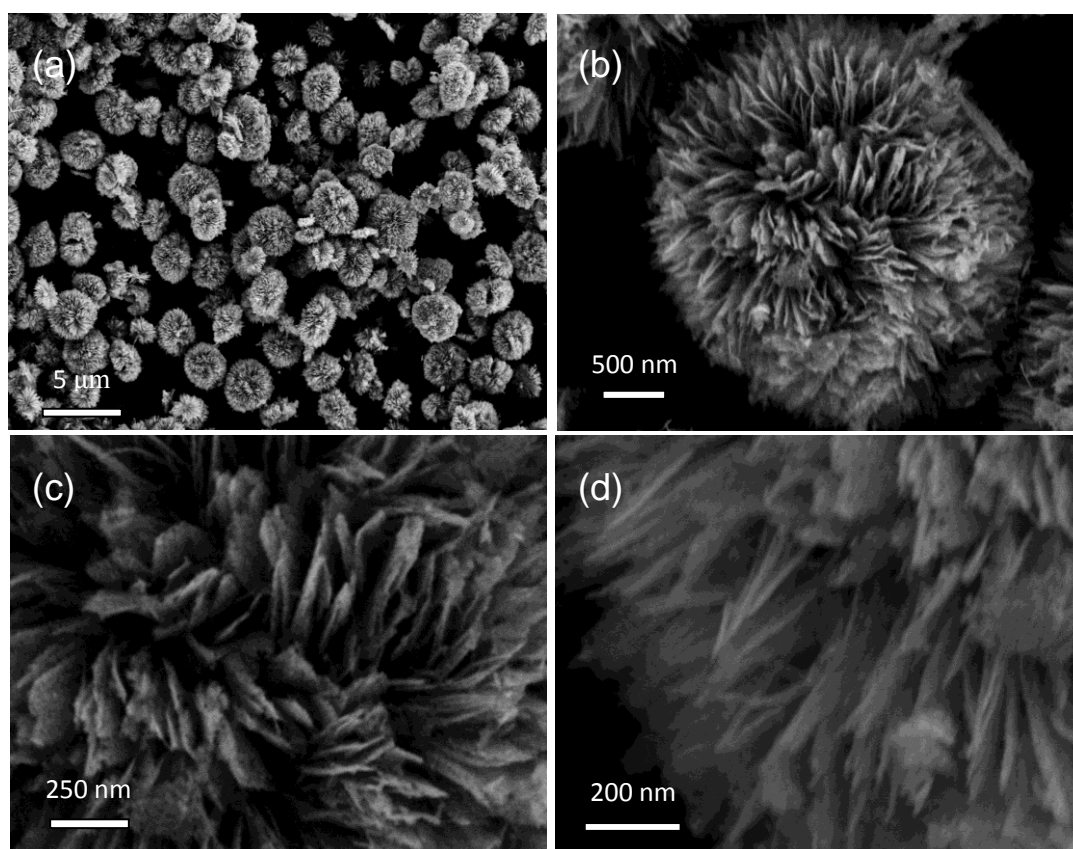


Figure 1 (a) The panoramic FESEM images of microsphere assembly of  $\text{TiO}_2$  nanosheets, (b)an representative microsphere assembly of  $\text{TiO}_2$  nanosheets, (c) enlarged FESEM view of the sheet-like structure, (d) further enlarged view showing the spinous structure of mesoporous  $\text{TiO}_2$  nanosheets.

Morphology and structure of the as-prepared microsphere assembly of mesoporous  $\text{TiO}_2$  nanosheets were investigated by field emission scanning electron microscope (FESEM) and shown in Figure 1. Figure 1a shows a panoramic FESEM image of the as-prepared  $\text{TiO}_2$  microsphere assembly of mesoporous  $\text{TiO}_2$  nanosheets. The obtained sample is well dispersed and exhibits a well-defined microspheric shape. The size of the microspheres is uniform with an average diameter of  $\sim 2 \mu\text{m}$ . The individual microsphere in Figure 1b is selected from Figure 1a, we can see that the surface of the microsphere has a thorn-like structure. Combined with the enlarged view of the microsphere surface in Figure 1c, there are a large number of spiny mesoporous nanosheets emanating from the central of the microsphere. A region of the microsphere is further magnified and shown in Figure 1d, it clearly displays that the spinous structure of  $\text{TiO}_2$  nanosheets are porous in the surface layers, the thickness of mesoporous  $\text{TiO}_2$  nanosheets is about 20 nm.

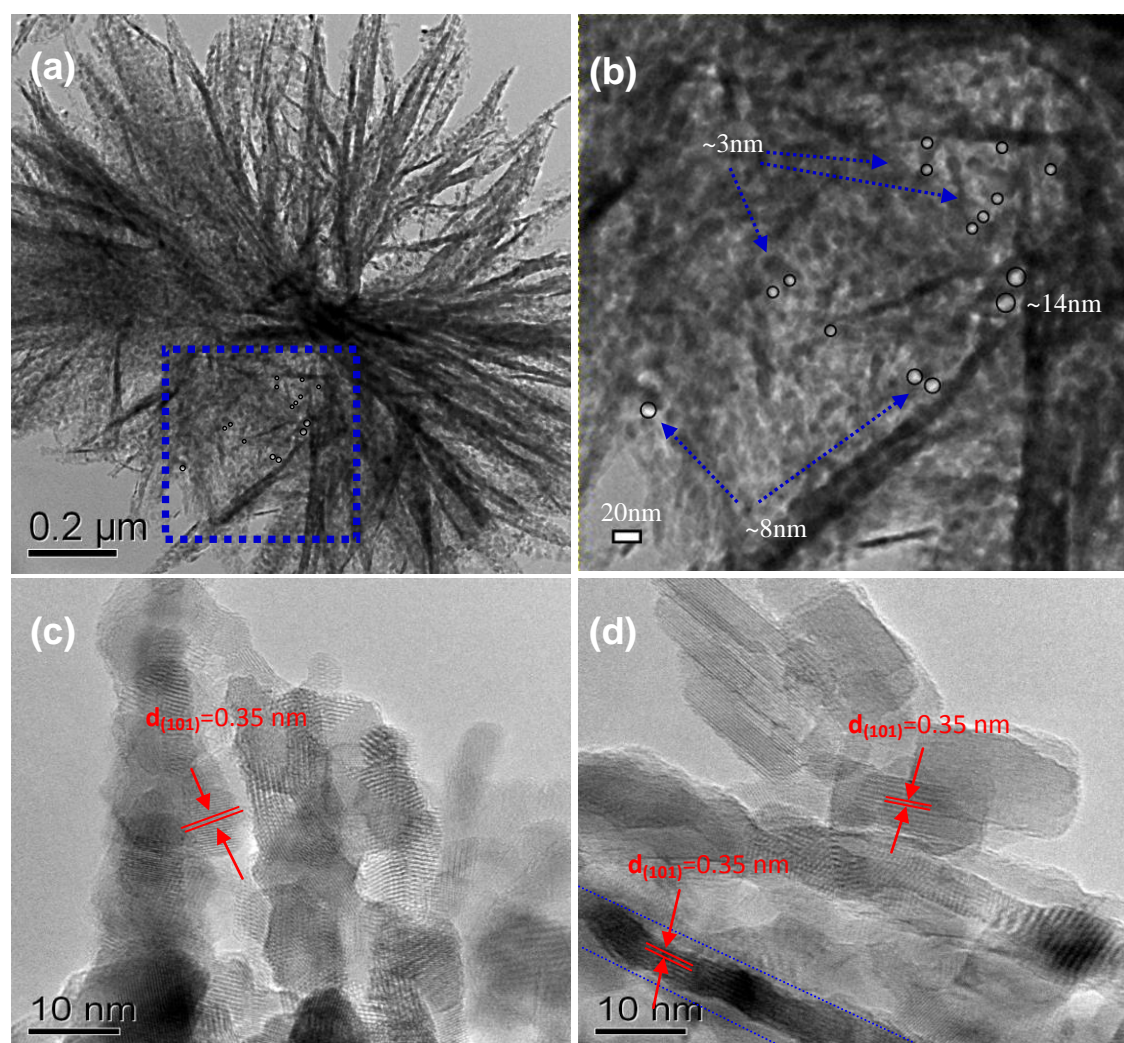


Figure 2 (a) TEM images of an individual microsphere of mesoporous  $\text{TiO}_2$  nanosheets, (b) the HRTEM enlarged images of mesoporous  $\text{TiO}_2$  nanosheets, (c) HRTEM of mesoporous  $\text{TiO}_2$  nanosheets,

(d) HRTEM of an individual mesoporous  $\text{TiO}_2$  nanosheet and  $\text{TiO}_2$  nanocuboids detached from the nanosheet.

The micro-nanostructures of spine hierarchical  $\text{TiO}_2$  microspheres were further examined by Transmission Electron Microscopy (TEM) and shown in Figure 2. Figure 2a reveals that there are a large number of  $\text{TiO}_2$  nanoparticles dispersed at the surface and inner of the thorn-like mesoporous nanosheet. In addition, amount of pores were exist in the nanosheets by careful observation. The diameter of the microsphere is about 2  $\mu\text{m}$  which is consistent with the SEM results. Figure 2b is the further enlarged HRTEM image of the blue square marked in Figure 2a, the mesoporous structure is distributed randomly in the  $\text{TiO}_2$  nanosheets. The diameter of the pore is mainly located at about 3 nm, 8 nm and 14 nm, which is consistent with the result of the nitrogen adsorption-desorption isotherms and the corresponding pore size distribution of the  $\text{TiO}_2$  microspheres in the following Figure 3. TEM image shows the microsphere is sparsely assembled by the thorn-like mesoporous  $\text{TiO}_2$  nanosheets. Figure 2c is the further enlarged HRTEM, from which we can see the lattice fringes of these small granules. The small regular cuboids in the thorn-like structure can be clearly seen in Figure 2c, it can be concluded that the thorn-like structure is formed by the assembly of these small regularly shaped nanocuboids. All the lattice spacing of these small cuboids is 0.35 nm, which corresponds to anatase  $\text{TiO}_2$  (101) crystal facet. HRTEM results indicate the (101) facet is exposed in the surface of mesoporous  $\text{TiO}_2$  nanosheets. Figure 2d is the HRTEM of an individual mesoporous  $\text{TiO}_2$  nanosheet and some nanocuboids detached from  $\text{TiO}_2$  nanosheet. The down left blue dotted area show  $\text{TiO}_2$  nanocuboids are in oriented attachment and formed single crystalline nanobelts, which serve as the rigid edge of mesoporous  $\text{TiO}_2$  nanosheet. Interestingly, some nanocuboids with length of  $\sim 20$  nm and width of  $\sim 10$  nm detached from  $\text{TiO}_2$  nanosheet were clearly observed in Figure 2d, which further confirm the building blocks of mesoporous nanosheet is  $\text{TiO}_2$  nanocuboids. According to SEM results, the thickness of the  $\text{TiO}_2$  mesoporous nanosheets is  $\sim 20$  nm. The lattice spacing of 0.35 nm shown in Figure 2d further confirms anatase  $\text{TiO}_2$  (101) crystal facet is mainly exposed in the surface of  $\text{TiO}_2$  nanocuboids building blocks. The lattice spacing of the (101) plane of the anatase phase may be directly related to the crystal growth of mesoporous  $\text{TiO}_2$  nanosheets. The adjacent anatase nanocuboids would coalesce in a way called “oriented attachment”, thus leading to the formation of anatase  $\text{TiO}_2$  nanosheets in [101] direction. This suggested that the oriented attachment occurred in the

[101] direction. In this case, the (101) plane is mainly exposed and beneficial for the dye absorption.<sup>31</sup>

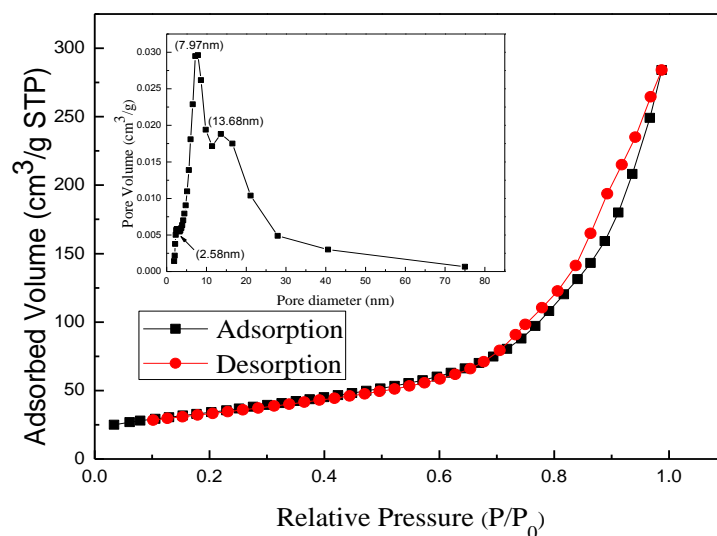


Figure 3 Nitrogen adsorption-desorption isotherms and the corresponding pore size distribution (inset) of the TiO<sub>2</sub> microspheres assembly of nanosheets.

To the further research into the porous structure and pore-size distribution of the as-obtained products, nitrogen adsorption-desorption isotherms are measured to ascertain the specific surface area and pore size of the TiO<sub>2</sub> microspheres. Figure 3 is the nitrogen adsorption-desorption isotherms of the TiO<sub>2</sub> microspheres assembly of TiO<sub>2</sub> nanosheets. The nitrogen adsorption-desorption isotherm of TiO<sub>2</sub> samples can be classified as types IV according to Brunauer-Deming-Deming-Teller (BDDT) classification.<sup>32</sup> The isotherm exhibits a linear absorption in the low range of relative pressure ( $< 0.7 P/P_0$ ). However, in the high relative pressure range of  $0.7\sim 1.0 P/P_0$ , the curve exhibits a hysteresis loop. The hysteresis observed in these isotherms is indicative of the existence of abundant mesoporous structures in the architectures according to IUPAC classification.<sup>33,34</sup> The plot of the pore-diameter distribution was determined by using the Barrett-Joyner-Halenda (BJH) method from the desorption branch of the isotherm. We find that the size of the pores is not uniform, inset of Figure 4 shows that TiO<sub>2</sub> nanosheets contain small pores (peak pore ca. 2.58 nm, 7.97 nm and 13.68 nm) and the BET surface area is  $123 \text{ m}^2 \text{ g}^{-1}$ .

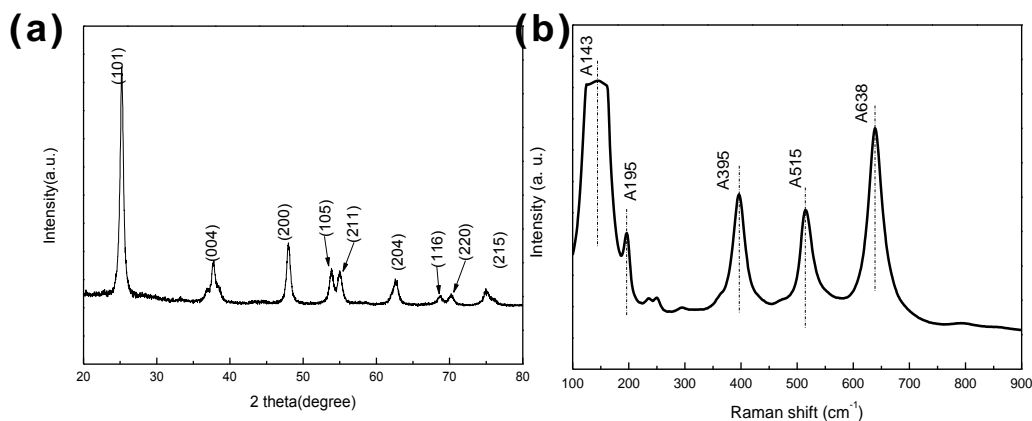


Figure 4 XRD patterns (a), and Raman spectra (b) of the microspheres of mesoporous TiO<sub>2</sub> nanosheets.

The phase compositions of the spiny hierarchical TiO<sub>2</sub> microspheres were examined by X-ray diffraction diffractometer and revealed in Figure 4a. Figure 4b is the Raman spectra of the TiO<sub>2</sub> microspheres. All the diffraction peaks in the XRD pattern can be guided to anatase TiO<sub>2</sub> (JPCDS file No.21-1272). As can be seen in Figure 4a, the characteristic peaks of the microspheres locate at the  $2\theta$  value of 25°, 37°, 48°, 54°, 55°, 63°, 69°, 70°, and 75°, which are corresponded to (101), (004), (200), (105), (211), (204), (116), (220), and (215) crystal planes of anatase TiO<sub>2</sub>, respectively.<sup>16,17</sup> TiO<sub>2</sub> nanocuboids in the [001] direction and the [100] direction can be evaluated from the full width at half-maximum of (004) and (200) diffraction peaks, respectively. The intensity of (004) diffraction peaks decreased in the XRD pattern of Figure 4a. This implied that crystal growth of the titania nanocuboids does not occurs along the [001] direction,<sup>34</sup> which further confirm the oriented attachment occurred in the [101] direction and is consistent with the TEM results. We all know that the XRD analysis gives the average thickness of the crystalline face stack, rather than the true lengths of the long and short axes that can be determined from the TEM images. The intensity of the (200) Bragg peaks was enhanced in Figure 4 when compared with (004) diffraction peaks, which means the thickness of the TiO<sub>2</sub> nanocuboids in the [100] direction was increased.<sup>35</sup> From the SEM observation, the thickness of the mesoporous TiO<sub>2</sub> nanosheets is about 20 nm.

Raman spectroscopy of the mesoporous TiO<sub>2</sub> nanosheets was shown in Figure 4b. All the peaks appearing at 143, 395, 515, and 638 cm<sup>-1</sup> were attributed to the typical anatase TiO<sub>2</sub> phase<sup>36</sup>. It has been known that the E<sub>g</sub> peak at 143 and 638 cm<sup>-1</sup> is mainly caused by symmetric stretching vibration of O–Ti–O of (101) crystalline facet in anatase TiO<sub>2</sub>, the B<sub>1g</sub> peak at 394 cm<sup>-1</sup> is caused by symmetric

bending vibration of O–Ti–O, while the  $A_{1g}$  peak at  $514\text{ cm}^{-1}$  is caused by antisymmetric bending vibration of O–Ti–O. The intensity of the  $A_{1g}$  ( $515\text{ cm}^{-1}$ ) and  $B_{1g}$  ( $395\text{ cm}^{-1}$ ) peaks in the Raman spectra increases when the (001) facets are highly exposed. On the contrary, the intensity of the  $E_g$  ( $143\text{ cm}^{-1}$  and  $638\text{ cm}^{-1}$ ) peaks were increasing, indicating that a high percentage of (101) facets were exposed<sup>35</sup>. The enhanced  $E_g$  peaks at  $143$  and  $638\text{ cm}^{-1}$  and the decrease of  $A_{1g}$  ( $515\text{ cm}^{-1}$ ) and  $B_{1g}$  ( $395\text{ cm}^{-1}$ ) peaks indicated the high percentage of exposed (101) facets, which were consistent with the TEM results and the following high dye absorption.

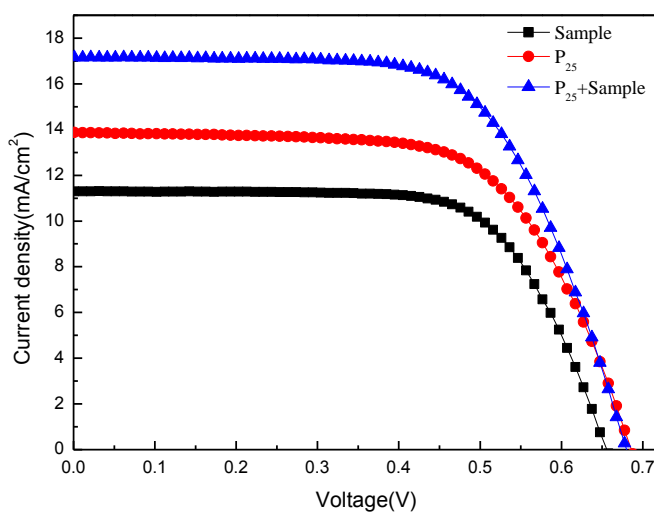


Figure 5 I-V curves of the quasi-solid-state DSSCs.

Table 1 Values of photovoltaic performance parameters for quasi-solid-state DSSCs.

DSSCs	$J_{sc}$ ( $\text{mA cm}^{-2}$ )	$V_{oc}$ (V)	FF	$\eta$ (%)	$C$ ( $10^{-7}\text{ mol/cm}^2$ )
$P_{25}$	13.86	0.69	0.64	6.11	0.93
Sample	11.58	0.64	0.69	5.15	1.33
$P_{25}$ +Sample	17.16	0.68	0.64	7.51	1.19

We fabricated three kinds of quasi-solid DSSC using the spine hierarchical  $\text{TiO}_2$  microspheres and commercial  $P_{25}$  particles as photoanode. The current (I)-voltage (V) curves were measured under a simulated solar light irradiation with an intensity of  $100\text{ mW}\cdot\text{cm}^{-2}$ . The results are shown in Figure 5 and the details are summarized in Table 1. As shown in Table 1, quasi-solid DSSC fabricated with  $P_{25}$  displays an open-circuit voltage of  $0.69\text{ V}$ , a short-circuit current density of  $13.86\text{ mA cm}^{-2}$ , and a fill

factor (FF) of 64 %, resulting in a light-to-electric energy conversion efficiency of 6.11%. Simultaneously, the quasi-solid-state DSSC based on spine hierarchical TiO<sub>2</sub> microspheres has a  $V_{oc}$ ,  $J_{sc}$ , FF, and  $\eta$  of 0.64 V, 11.58 mA cm<sup>-2</sup>, 69%, and 5.15%, respectively. The obtained micro-sized sample shows a slightly low conversion efficiency than that of P<sub>25</sub> nanoparticles due to its larger diameter (2  $\mu$ m) hindering the electron transfer, which is further confirmed by the following EIS investigation. Interestingly, the dye absorption of the obtained TiO<sub>2</sub> microsphere is higher than that of P<sub>25</sub>. It is well-known that the dye absorption ability of anatase TiO<sub>2</sub> (101) facets is the highest among all the crystalline facets.<sup>37, 38</sup> The higher dye loading is mainly attributed to the highly exposed (101) facet and the mesoporous structure. Thus, the microsphere of TiO<sub>2</sub> mesoporous nanosheets is a good candidate for the light scattering materials. A better photovoltaic performance was achieved by using the sample as a top scattering layer. The optimized solar cell obtained an open-circuit voltage of 0.68 V, a short-circuit current density ( $J_{sc}$ ) of 17.16 mA cm<sup>-2</sup>, a fill factor of 64% and a higher light-to-electric energy conversion efficiency of 7.51%. The optimized solar cell shows a 45.8 percent increase in overall conversion efficiency compared with the microsphere of TiO<sub>2</sub> mesoporous nanosheets.

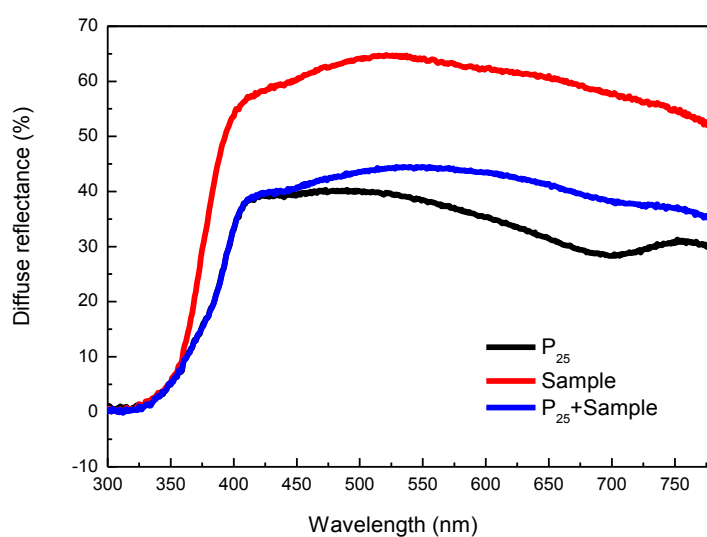


Figure 6 UV-vis diffuse reflectance spectra of the different TiO<sub>2</sub> films.

Figure 6 shows the UV-vis diffuse reflectance spectra of different TiO<sub>2</sub> photoanode films. The curve apparently shows the reflectance spectra of microsphere assembly of mesoporous TiO<sub>2</sub> nanosheets film is much higher than that of commercial P<sub>25</sub> film in the near-infrared regions and visible light regions from 400 nm to 800 nm. Furthermore, the light scattering ability of the DSSC was improved when introducing the microsphere assembly of mesoporous TiO<sub>2</sub> nanosheets as the top scattering layer. The

optical path of the incident light in the DSSC was increased and got better light capture efficiency owing to the higher diffuse capacity of the obtained micro-sized samples and the sheet-like structure. When the incident light collides with TiO<sub>2</sub> microsphere, the light scatters strongly, which increases the light path length in the TiO<sub>2</sub> films and enhanced the chance of dye sensitizer contacting with the incident light, thus finally improve the performance of the solar cell.

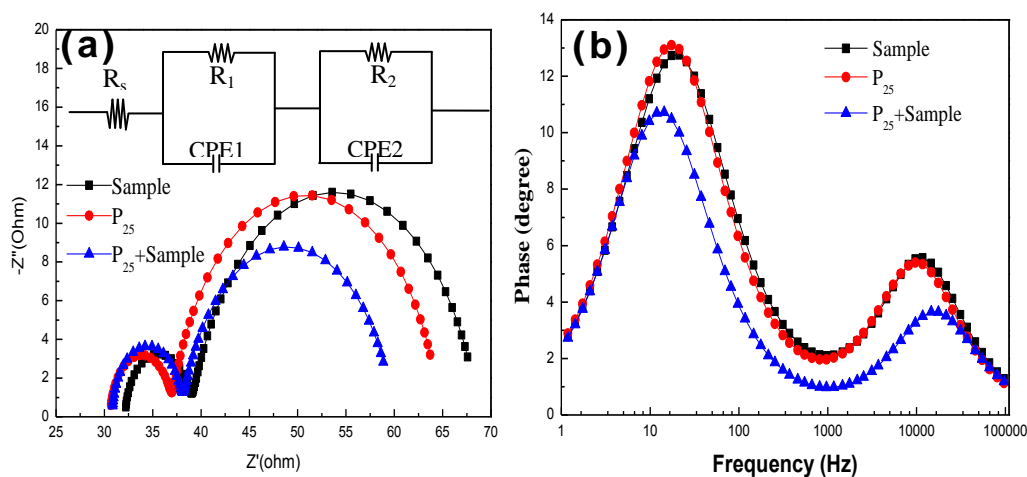


Figure 7 EIS spectra (a) and bode phase plots (b) of the quasi-solid-state DSSCs, inset of (a) is the equivalent circuit model.

Table 2. Electron lifetime ( $\tau_r$ ) of the DSSCs based on different electrodes.

DSSC	Phase (degree)	Frequency (Hz)	$\tau_r$ (ms)
Sample	12.75	21.23	7.50
P <sub>25</sub>	13.10	17.44	9.13
P <sub>25</sub> +Sample	9.23	14.36	11.09

The EIS measurement has been regarded as a helpful technique to investigate the kinetics of electrochemical and the charge transfer process of DSSCs. The charge transfer at Pt counter electrode, electron transfer and recombination in TiO<sub>2</sub> photoanode films and the diffusion of redox couples in the electrolyte solution can be surveyed by the EIS spectra.<sup>39,40</sup> In a general way, the small semi-circle in the high frequency region is laid to the redox reaction between the electrolyte and Pt interface. The large semi-circle in the middle frequency is ascribed to electron transfer at the interface of TiO<sub>2</sub>/dye/electrolyte.<sup>41</sup> The insert of Fig. 7a is the equivalent circuit model that had been used to optimize the obtained EIS polts by using ZsimDemo 3.20 software. The electron transfer resistance at

the interface of TiO<sub>2</sub>/dye/electrolyte for the spine TiO<sub>2</sub> microspheres is larger than that of P<sub>25</sub> nanocrystalline, which causing a low current applied in quasi-solid-state DSSCs. The electron transfer at the interface of TiO<sub>2</sub>/dye/electrolyte for the spine TiO<sub>2</sub> microspheres using as a scattering layer is smaller than that of P<sub>25</sub> nanocrystalline and the obtained sample, which implies that the bi-layer structure of the photoanode reduces the charge transfer resistance at the TiO<sub>2</sub>/dye/electrolyte interface. The reason is possibly that the TiO<sub>2</sub> microsphere is beneficial for the infiltration of the quasi-solid quasi-solid-state electrolyte.

Figure 7b displays Bode phase plots corresponding to the EIS results. Frequencies of the two peaks from high to low frequency region are the characteristic representative of the charge transfer of electrodes and TiO<sub>2</sub>/dye/electrolyte interface, respectively. The electron lifetime ( $\tau_r$ ) of the DSSCs were calculated according to the following equation:

$$\tau_r = \frac{1}{2\pi f_{\max}} \quad (2)$$

Where  $f_{\max}$  signifies the maximum frequency of the frequency peak.<sup>42</sup> The results were listed in table 2. The higher values of  $\tau_r$  mean the electron recombination reaction between photo-generated electrons and I<sub>3</sub><sup>-</sup> is effectively blocked. From table 2, the electron lifetime ( $\tau_r$ ) of the bi-layer structured device is 11.09 ms, which is higher than the P<sub>25</sub> of 9.13 ms, demonstrating the weak charge recombination in the double layer and the effective electron transfer when compared with P<sub>25</sub>. As is well known, the extended electron lifetime is beneficial for DSSC to achieve better power-conversion efficiency.

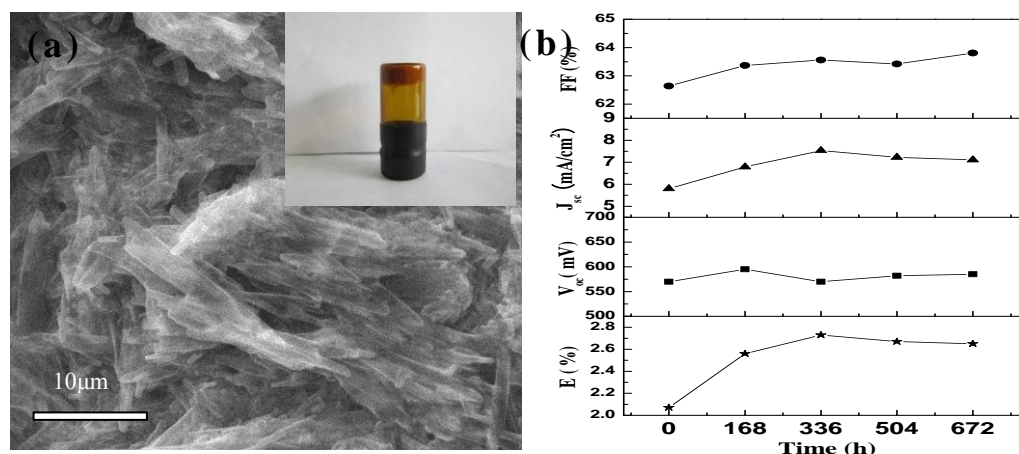


Figure 8 (a) SEM image of quasi-solid-state electrolyte, upper inset is the picture of the inverted electrolyte showing the solid characteristics, (b) Stability test of the QDSSC.

Figure 8a displays the SEM image of quasi-solid state electrolyte prepared by adding an appropriate amount of 4-cyano-4'-heptyloxy biphenyl into the liquid electrolyte. As can be seen from

the SEM image, the mixed electrolyte solution showed rod-like structure when 4-cyano-4'-heptyloxy biphenyl was added. The rod-like structure in the electrolyte leads to the liquid electrolyte solution turning into solid state electrolyte. The upper inset in Figure 8a is the physical digital photo of quasi-solid state electrolyte. The picture shows the liquid crystal electrolyte does not flow downward after inversion, indicating that the electrolyte has been cured into solid state. In order to study the stability of quasi-solid electrolyte for dye-sensitized solar cell, encapsulated battery with a large area of 2 cm \* 2 cm is placed under natural conditions for a month to test its photovoltaic properties every week. The change of photovoltaic parameters with the time is plotted in Figure 8b, the efficiency of the cell is low at the beginning, since the solid electrolyte does not fully penetrate into the film. The battery performance increased with the time increase and the parameters stabilized after four weeks, indicating a good stability of quasi-solid electrolyte in the natural environment.

#### 4. Conclusion

In summary, we prepared a novel type of microsphere organization of TiO<sub>2</sub> mesoporous nanosheets via a one-step hydrothermal method. The anatase TiO<sub>2</sub> microspheres were monodispersed, the building block of the microsphere is mesoporous TiO<sub>2</sub> nanosheets. TiO<sub>2</sub> mesoporous nanosheets were further assembled by crystalline anatase nanocuboids with (101) facet highly exposed in the surface. Considering the excellent light scattering and dye absorption property of the hierarchical microspheres, we prepared a double-layer photoanode using the microspheres as the top light-scattering layer. In addition, the solidified electrolyte was prepared by adding liquid crystal of 4-cyano-4'-heptyloxy biphenyl into electrolyte solution. The quasi-solid-state DSSC using the spine hierarchical TiO<sub>2</sub> microspheres as the top light-scattering layer obtained a power conversion efficiency of 7.51%. The research results display that the spine hierarchical microsphere of TiO<sub>2</sub> mesoporous nanosheets has a potential application in quasi-solid-state dye-sensitized solar cells with an excellent stability.

#### Acknowledgment

This research was supported by the Natural Science Foundation of China (No. U1162108, No. 51272104); the Natural Science Foundation of Jiangsu Province Office of Education (BK20131409), Natural Science Foundation of the Jiangsu Higher Education Institutions of China (No.11KJA150002),

Qing Lan project of Jiangsu Province, the Financial Foundation of State Key Laboratory of Materials-Oriented Chemical Engineering and A Project Funded by the Priority Academic Program Development of Jiangsu Higher Education Institutions.

## References

1. T. V. Arjunan and T. S. Senthil, *Materials Technology* 2013, **28**, 9-14.
2. A. Bahrami, S. Mohammadnejad, and S. Soleimaninezhad, *Opt. Quant. Electron.* 2013, **45**, 161-197.
3. B. O'Regan, and M. Grätzel, *Nature* 1991, **353**, 737-740.
4. D. Kim, A. Ghicov, S. P. Albu, and P. Schmuki, *J. Am. Chem. Soc.* 2008, **130**, 16454-16455.
5. I. Chung, B. H. Lee, J. Q. He, R. P. H. Chang, and M. G. Kanatzidis, *Nature* 2012, **485**, 486-490.
6. H. C. Sun, Y. H. Luo, Y. D. Zhang, D. M. Li, Z. X. Yu, K. X. Li, and Q. B. Meng, *J. Phys. Chem. C* 2010, **114**, 11673-11679.
7. N. Q. Fu, X. R. Xiao, X. W. Zhou, J. B. Zhang, and Y. Lin, *J. Phys. Chem. C* 2012, **116**, 2850-2857.
8. N. Q. Fu, Y. Y. Fang, Y. D. Duan, X. W. Zhou, X. R. Xiao, and Y. Lin, *ACS Nano* 2012, **6**, 9596-9605.
9. S. M. Sawanta, A. B. Chirayath, N. B. Popatrao, S. S. Pravin, M. R. Pramod, R. J. Sandesh, and S. P. Pramod, *CrystEngComm.* 2012, **14**, 8156-8161.
10. F. Sauvage, J. D. Decoppet, M. Zhang, S. M. Zakeeruddin, P. Comte, M. Nazeeruddin, P. Wang, and M. Grätzel, *J. Am. Chem. Soc.* 2011, **133** (24), 9304-9310.
11. X. Zhang, F. Liu, Q. L. Huang, G. Zhou, and Z. S. Wang, *J. Phys. Chem. C* 2011, **115**, 12665-12671.
12. E. Ramasamy, and J. Lee, *Chem. Commun.* 2010, **46**, 2136-2138.
13. S. Y. Lee, B. Yoo, M. K. Lim, T. Lee, A. R. S. Priya, and K. Kim, *Langmuir* 2010, **26**, 6638-6642.
14. M. Quintana, T. Edvinsson, A. Hagfeldt, and G. Boschloo, *J. Phys. Chem. C* 2007, **111**, 1035-1041.
15. Q. Hu, C. C. Wu, L. Q. Cao, B. Chi, J. Pu, and L. Jian, *J. Power Sources* 2013, **226**, 8-15.
16. T. Ling, J. G. Song, X. Y. Chen, J. Yang, S. Z. Qiao, and X. W. Du, *J. Alloys Compd.* 2013, **546**, 307-313.

17. K. Kim, S. Lee, D. Kima, D. Hwang, and Y. Heo, *Curr. Appl. Phys.* 2013, **13**, 795-798.
18. B. Chen, and K. Lu, *Langmuir* 2012, **28**, 2937-2943.
19. Z. H. Liu, X. J. Su, G. L. Hou, S. Bi, Z. Xiao, and H. P. Jia, *J. Alloys Compd.* 2013, **555**, 68-73.
20. H. P. Wu, C. M. Lan, J. Y. Hu, W. K. Huang, J. W. Shiu, Z. J. Lan, C. M. Tsai, C. H. Su and E. W. Diau, *J. Phys. Chem. Lett.* 2013, **4**, 1570-1577.
21. X. H. Sun, Y. M. Liu, Q. D. Tai, B. L. Chen, T. Peng, N. Huang, S. Xu, T. Y. Peng, and X. Z. Zhao, *J. Phys. Chem. C* 2012, **116**, 11859-11866.
22. Z. F. Zhu, C. K. Zhu, H. Liu, Y. F. Wu, G. H. Chen, T. Lv, *Appl. Surf. Sci.* 2014, 308, 301-305.
23. M. Zukulova, A. Zukal, L. Kavan, M. K. Nazeeruddin, P. Liska, and M. Grätzel, *Nano Lett.* 2005, **5** (9), 1788-1792.
24. D. P. Wu, F. Zhu, J. M. Li, H. Dong, Q. Li, K. Jiang, and D. S. Xu, *J. Mater. Chem.* 2012, **22**, 11665-11671.
25. G. T. Dai, L. Zhao, J. Li, L. Wan, F. Hu, Z. X. Xu, B. H. Dong, H. B. Lu, S. M. Wang, and J. G. Yu, *J. Colloid Interf. Sci.* 2012, **365**, 46-52.
26. G. T. Dai, L. Zhao, S. M. Wang, J. H. Hu, B. H. Dong, H. B. Lu, and J. Li, *J. Alloys Compd.* 2012, **539**, 264-270.
27. H. Tao, W. P. Chen, J. Wang, W. J. Ke, J. W. Wan, J. H. Wu, and G. J. Fang, *Electrochimica Acta* 2014, **137**, 17-25.
28. A. Yella, H. Lee, H. N. Tsao, C. Y. Yi, A. K. Chandiran, M. K. Nazeeruddin, E. W. Diau, C. Yeh, S. M. Zakeeruddin, and M. Grätzel, *Science* 2011, **334**, 629-634.
29. M. S. Kang, K. S. Ahn, and J. W. Lee, *J. Power Sources* 2008, **180**, 896-901.
30. M. Wang, X. Pan, X. Q. Fang, L. Guo, W. Q. Liu, C. N. Zhang, Y. Huang, L. H. Hu, and S. Y. Dai, *Adv. Mater.* 2010, **22**, 5526-5530.
31. M. Adachi, Y. Murata, J. Takao, J. T. Jiu, M. Sakamoto, and F. M. Wang, *J. Am. Chem. Soc.* 2004, **126**, 14943-14949.
32. J. G. Yu, J. J. Fan, and K. L. Lv, *Nanoscale* 2010, **2**, 2144-2149.
33. K. M. Guo, M. Y. Li, X. L. Fang, L. H. Bai, M. D. Luoshan, F. P. Zhang, and X. Z. Zhao, *J. Power Sources* 2014, **264**, 35-41.
34. Q. J. Xiang, K. L. Lv, and J. G. Yu, *Appl. Catal. B* 2010, **96**, 557-564.
35. F. Tian, Y. P. Zhang, J. Zhang, and C. X. Pan, *J. Phys. Chem. C* 2012, 116, 7515-7519.

36. O. Frank, M. Zukalova, B. Laskova, J. Kuerti, J. Koltai, and L. Kavan, *Phys. Chem. Chem. Phys.* 2012, **14**, 14567-14572
37. Y. Zhou, X. Y. Wang, H. Wang, Y. P. Song, L. Fang, N. Q. Ye and L. J. Wang, *Dalton Trans.* 2014, **43**, 4711-4719
38. P. Joshi, L. F. Zhang, D. Davoux, Z. T. Zhu, D. Galipeau, H. Fong, and Q. Q. Qiao, *Energy Environ. Sci.* 2010, **3**, 1507-1510.
39. F. Fabregat-Santiago, J. Bisquert, E. Palomares, L. Otero, D. B. Kuang, S. M. Zakeeruddin, and M. Grätzel, *J. Phys. Chem. C* 2007, **111**, 6550-6560.
40. M. Adachi, M. Sakamoto, J. T. Jiu, Y. Ogata, and S. Isoda, *J. Phys. Chem. B* 2006, **110**, 13872-13880.
41. W. G. Yang, F. R. Wan, Q. W. Chen, J. J. Li, and D. S. Xu, *J. Mater. Chem.* 2010, **20**, 2870-2876.